Solid-State Electronics 52 (2008) 1791–1795

Contents lists available at ScienceDirect

Solid-State Electronics

journal homepage: www.elsevier.com/locate/sse

Normally-Off AlGaN/GaN HEMTs with InGaN cap layer: A simulation study

S. Vitanov *, V. Palankovski

Advanced Material and Device Analysis Group, Institute for Microelectronics, TU Vienna, Austria

ARTICLE INFO

Article history:
Received 19 June 2008
Accepted 22 July 2008
Available online 17 September 2008

The review of this paper was arranged by Prof. A. Zaslavsky

Keywords:
Simulation
HEMT
Enhancement mode
InGaN
Modeling

ABSTRACT

AlGaN/GaN high electron mobility transistors (HEMTs) are favored for the use in high-power and high-frequency applications. Normally-off operation has been desired for various applications, but proved to be difficult to achieve. Recently, a new approach was proposed by Mizutani et al. [Mizutani T, Ito M, Kishimoto S, Nakamura F. AlGaN/GaN HEMTs with thin InGaN cap layer for normally-off operation. IEEE Elec Dev Lett 2007;28(7):549–51]: a thin InGaN cap layer introduces a polarization field, which raises the conduction band of the AlGaN/GaN interface. As a result, the threshold voltage is shifted in positive direction. Relying on the experimental work of Mizutani et al. we conduct a simulation study of the proposed devices. Our device simulation tool is expanded by material models for InN and InGaN and also an improved high-field mobility model accounting for the specifics of the III-N materials. Using this setup, we further explore the device specific effects and conduct an analysis of the AC characteristics.

1. Introduction

As AlGaN/GaN depletion mode (D-mode) HEMT technology has been significantly improved in the recent years, no comparable progress of the enhancement counterparts (E-mode) could be noted. However, the latter exhibit features, which give them advantages over traditional D-mode HEMTs in some applications. In low-power digital circuitry they allow HEMT-based direct-coupled FET logic. In analog circuits they offer reduced complexity due to the elimination of the negative voltage supply and fail-safe power-switching. Several groups have proposed different approaches to the design of E-mode HEMTs in the past years. Khan et al. described a device featuring very thin AlGaN barrier layer with a threshold voltage $V_{th} = 50$ mV and $g_m = 23$ mS/mm [2]. Kumar et al. reported $V_{th} = 75$ mV and $f_T = 8$ GHz for a recessed gate device [3]. Cai et al. relied on fluoride-based plasma treatment to achieve a threshold voltage $V_{th} = 900$ mV, $g_m = 148$ mS/mm, and $f_T = 10$ GHz [4]. While the last method delivers excellent results, stability concerns remain. The most recent approach (proposed by Mizutani et al.) adopts a thin InGaN cap layer, which raises the conduction band, thereby achieving a normally-off operation [1].

In this work, we study structures incorporating InGaN cap layer by the means of two-dimensional numerical device simulation. The material models employed for GaN and InN are described. Relevant physical effects are accounted for, such as thermionic field emission, self-heating, etc. Also an improved high-field mobility model considering the specifics of the III-N materials is employed. After an initial calibration against the DC characteristics of a traditional device as reported by Mizutani et al., we discuss the peculiarities of the recessed structure and perform AC analysis.

2. Device structure

The investigated InGaN/AlGaN/GaN device structure as described in [1] is shown in Fig. 1. A 3 μm thick GaN layer is grown on a sapphire substrate. A 20 nm thick $Al_{0.25}Ga_{0.75}N$ layer is deposited next: the first 5 nm undoped, 10 nm highly doped (2×10^{18} cm^{-3}) supply layer, and 5 nm undoped material. On-top a 5 nm thick $In_{0.2}Ga_{0.8}N$ layer is deposited. All layers are non-intentionally doped, except the supply layer. The gate length $l_g = 1.9$ μm, source-gate distance is 1.5 μm, and gate-drain distance is 2.4 μm. We study three different HEMT structures: the proposed novel normally-off device (Fig. 1), a device with the InGaN layer removed in the access regions (only the InGaN film under the gate is left), and a conventional normally-on device (as in Fig. 1, but without the InGaN layer). We assume a diffusion of the metal source and drain contacts reaching the highly doped layer.

* Corresponding author. Tel.: +43 1 58801 36038; fax: +43 1 58801 36099.
E-mail addresses: vitanov@iue.tuwien.ac.at (S. Vitanov), palankovski@iue.tuwien.ac.at (V. Palankovski).

0038-1101/$ - see front matter © 2008 Elsevier Ltd. All rights reserved.
doi:10.1016/j.sse.2008.07.011

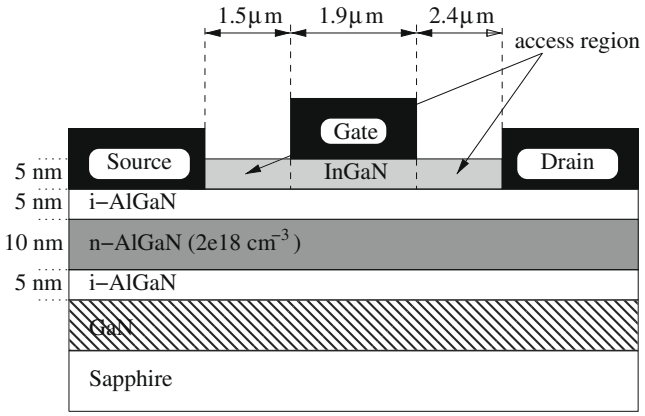

Fig. 1. Schematic layer structure of the three HEMTs under investigation.

3. Physical and material models

Our two-dimensional device simulator MINIMOS-NT [5] has proven to be a suitable tool for the analysis of heterostructure devices [6]. Recently, it has been used for the study of a whole generation of AlGaN/GaN-based HEMTs [7]. Since the longitudinal electric field in the channel reaches peak values of above 500 kV/cm, the hydrodynamic transport model is used to properly model electron transport and energy relaxation. Self-heating effects are accounted for by using a global self-heating model, which calculates a spatially constant lattice temperature. This model has been chosen for the reasonable computational effort and convergence behavior. We further assess the impact of thermionic emission and field emission (tunneling) effects which determine the current transport across the heterojunctions. The energy barrier reduction is modeled based on the electric field perpendicular to the interface and the effective tunneling length [8].

3.1. Semiconductor equations

The basic equations solved in a device simulator are the Poisson equation and the current continuity equations for electrons and holes (1)–(3). The unknown quantities are the electrostatic potential ψ and the electron and hole concentration n and p. C_{net} denotes the net concentration of the ionized dopants, ε is the dielectric permittivity of the semiconductor, and R is the net recombination rate. E_C and E_V are the position-dependant band energies, $N_{C,0}$ and $N_{V,0}$ the effective density of states, and μ_n and μ_p are the carrier mobilities. The basic equations are completed through two additional equations describing the conservation of the average carrier energies, (4) and (5). T_n and T_p denote the carrier temperatures, $\tau_{w,n}$ and $\tau_{w,p}$ are the energy relaxation times, $\mathbf{S}_n$ and $\mathbf{S}_p$ the energy fluxes, $\mathbf{J}_n$ and $\mathbf{J}_p$ the carrier current densities.

$$\operatorname{div}(\varepsilon \cdot \operatorname{grad}\psi) = q \cdot (n - p - C_{\text{net}}) \tag{1}$$

$$\operatorname{div}\left(\mu_n \cdot n \cdot \left(\operatorname{grad}\left(\frac{E_C}{q} - \psi\right) + \frac{k_B}{q} \cdot \frac{N_{C,0}}{n} \cdot \operatorname{grad}\left(\frac{n \cdot T_n}{N_{C,0}}\right)\right)\right) = R + \frac{\partial n}{\partial t} \tag{2}$$

$$\operatorname{div}\left(\mu_p \cdot p \cdot \left(\operatorname{grad}\left(\frac{E_V}{q} - \psi\right) - \frac{k_B}{q} \cdot \frac{N_{V,0}}{p} \cdot \operatorname{grad}\left(\frac{p \cdot T_p}{N_{V,0}}\right)\right)\right) = R + \frac{\partial p}{\partial t} \tag{3}$$

$$\operatorname{div}\,\mathbf{S}_n = \operatorname{grad}\left(\frac{E_C}{q} - \psi\right) \cdot \mathbf{J}_n - \frac{3 \cdot k_B}{2} \cdot \left(\frac{\partial(n \cdot T_n)}{\partial t} + R \cdot T_n + n \cdot \frac{T_n - T_L}{\tau_{w,n}}\right) \tag{4}$$

$$\operatorname{div}\,\mathbf{S}_p = \operatorname{grad}\left(\frac{E_V}{q} - \psi\right) \cdot \mathbf{J}_p - \frac{3 \cdot k_B}{2} \cdot \left(\frac{\partial(p \cdot T_p)}{\partial t} + R \cdot T_p + p \cdot \frac{T_p - T_L}{\tau_{w,p}}\right) \tag{5}$$

Since HEMTs are unipolar devices, computational effort can be reduced by neglecting the equations for holes (3) and (5). The system of differential equations is solved self-consistently. The material parameters, such as dielectric constant, band energies, carrier mobilities, and energy relaxation times, are properly modeled.

3.2. Band structure

While the band structure of GaN has been studied profoundly, recent reports have questioned the alleged bandgap of 1.89 eV for InN. Therefore, the band structure and electron mass had to be reconsidered. Table 1 summarizes the values of the bandgap at 0 K ($E_{g,0}$), electron mass (m_n), and dielectric constant (ε_r) for GaN and InN. The resulting parameters for $In_xGa_{1-x}N$ are linearly interpolated, except for the bandgap. The temperature dependence of the bandgap is calculated first by

$$E_g = E_{g,0} - \frac{\alpha_g T_L^2}{\beta_g + T_L} \tag{6}$$

with Varshni parameters for GaN [9] and InN [10] as shown in Table 1. The bandgap of $In_xGa_{1-x}N$ is then interpolated by

$$E_g^{\text{InGaN}} = E_g^{\text{InN}}(1-x) + E_g^{\text{GaN}}x + C_g(1-x)x \tag{7}$$

with a bowing parameter C_g =1.4 eV in agreement with Walukievicz et al. [10]. An energy offset (E_{off}) is used to align the valence band of different materials. For $In_xGa_{1-x}N$ it is calculated by

$$E_{\text{off}}^{\text{InGaN}} = \frac{E_{\text{off}}^{\text{InN}}(E_g^{\text{InGaN}} - E_g^{\text{GaN}}) - E_{\text{off}}^{\text{GaN}}(E_g^{\text{InGaN}} - E_g^{\text{InN}})}{E_g^{\text{InN}} - E_g^{\text{GaN}}} \tag{8}$$

where the offset energies for GaN and InN are $E_{\text{off}}^{\text{GaN}} = 0.0$ eV and $E_{\text{off}}^{\text{InN}} = 1.05$ eV, respectively (the valence band edge of GaN is chosen as reference) [6]. The barrier height of the Schottky contact to AlGaN is 1.5 eV [11] and 0.5 eV to InGaN [12], respectively.

3.3. Mobility model

The low-field electron mobility μ^{LI} is modeled using the expression proposed by Caughey and Thomas [13] with coefficients which depend on the lattice temperature T_L:

$$\mu^{\text{LI}} = \mu^{\min} + \frac{\mu^{L} - \mu^{\min}}{1 + \left(C_I / C^{\text{ref}}\right)^{\gamma_0}}, \quad \text{where} \tag{9}$$

$\mu^{L} = \mu_{300}^{L}\left(\frac{T_L}{300K}\right)^{\gamma_1}$, $\mu^{\min} = \mu_{300}^{\min}\left(\frac{T_L}{300K}\right)^{\gamma_1}$, and $C^{\text{ref}} = C_{300}^{\text{ref}}\left(\frac{T_L}{300\ K}\right)^{\gamma_2} \cdot C_I$ denotes the concentration of ionized impurities. Figs. 2–4 compare the models for GaN and InN to our Monte Carlo (MC) simulation results and experimental data as a function of free carrier concentration and lattice temperature T_L. The model for GaN is calibrated against the MC data [14], which exhibits a mobility slightly higher than suggested by most experimental results. The latter show increasing values in recent years, due to the improved quality of the material samples. The model for InN is calibrated against a MC simulation, which assumes the newly proposed bandgap of $\approx$ 0.7 eV at approx. 300 K and proper band structure and electron masses [15]. The calibrated model parameter values are listed in Table 2. The low-field mobility (μ^{LI}) of $In_xGa_{1-x}N$ is then calculated by a harmonic mean:

Table 1
Summary of band structure parameters

Material	$E_{g,0}$ (eV)	α_g ($\times 10^{-4}$ eV/K)	β_g (K)	m_n	ε_r
GaN	3.4	9.09	800	$0.2m_0$	8.9
InN	0.9	4.14	454	$0.04m_0$	15.3

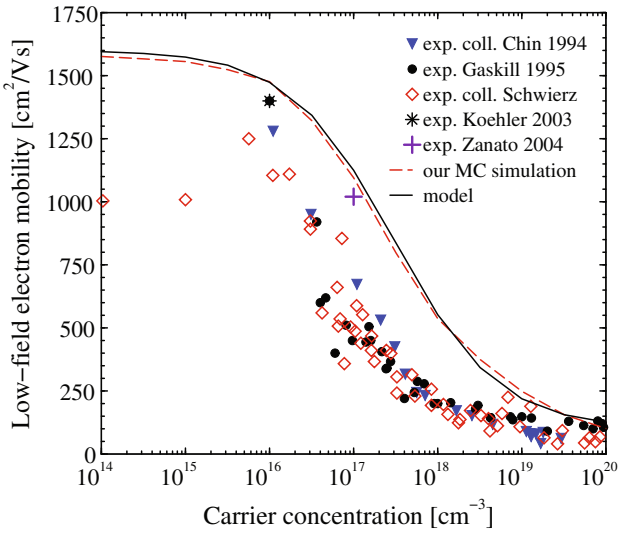

Fig. 2. Electron mobility versus concentration in GaN: experimental data, MC simulation results and model used in the device simulator.

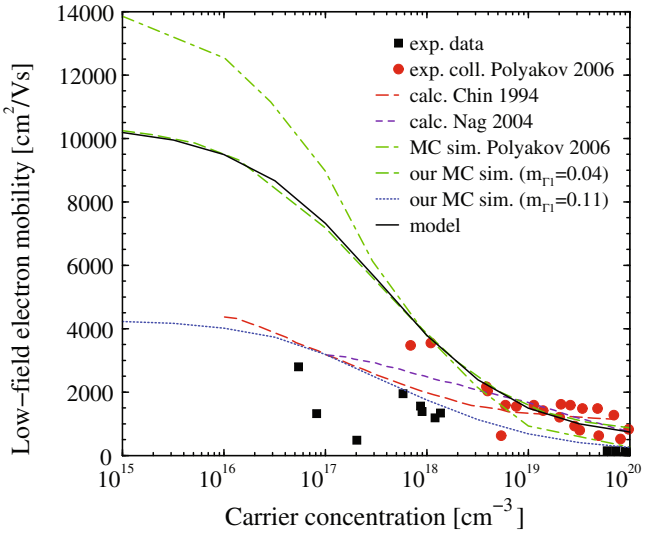

Fig. 3. Electron mobility versus concentration in InN: experimental data, MC simulation results and model used in the device simulator.

$$\frac{1}{\mu^{\mathrm{InGaN}}} = \frac{1-x}{\mu^{\mathrm{InN}}} + \frac{x}{\mu^{\mathrm{GaN}}} \tag{10}$$

The high-field mobility model includes energy-dependent electron relaxation times. A modified hydrodynamic mobility model (based on the one proposed by Hänsch et al. [16]), which accounts for specific effects of GaN-based materials [17] is used:

$$\mu^{\mathrm{LIT}} = \frac{\mu^{\mathrm{LI}}(T_n/T_L)^{\gamma}}{\left(1+\alpha^{1/\beta}(T_n-T_L)^{1/\beta}\right)^{\beta}}, \quad \text{where} \quad \alpha = \frac{3k_B\mu^{\mathrm{LI}}}{2q\tau_{w,n}(v_{sat})^2}. \tag{11}$$

T_n is the electron temperature, $\tau_{w,n}$ are the energy-dependent relaxation times [14]. The latter is modeled with temperature dependence as given in [6]. v_{sat} is the saturation velocity. From the values for GaN and InN (see Table 2), the saturation velocity for $In_xGa_{1-x}N$ is linearly interpolated. The parameter β is used to model the mobility for moderate carrier temperatures. The parameter γ models the decay of the electron velocity in GaN, AlGaN, and InGaN at high electron temperatures. The conventional Hänsch model corresponds to the $\beta = 1$, $\gamma = 0$ parameter set. Higher β values result in lower peak velocity, while negative γ values decrease the velocity at higher electric fields. We choose a set with $\beta = 1.2$, $\gamma = -0.5$.

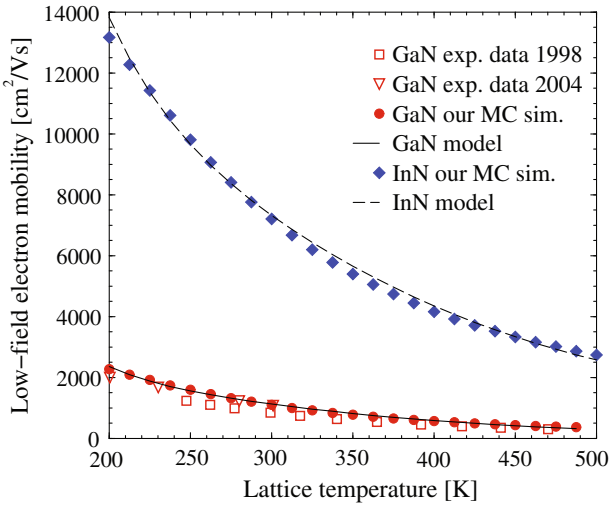

Fig. 4. Low-field electron mobility as a function of lattice temperature at carrier concentration of 10^{17}cm^{-3}.

Table 2
Summary of electron transport parameters

Material	μ^{L}_{300} (cm²/Vs)	μ^{min}_{300} (cm²/Vs)	C^{ref}_{300} ($\times 10^{17}$ cm^{-3})	γ_0 (–)	γ_1 (–)	γ_2 (–)	v_{sat} (cm/s)
GaN	1600	100	3	0.7	−3.0	4.4	10^7
InN	10400	500	3.4	0.65	−2.7	4.5	1.5×10^7

4. Simulation results

The simulation results for the transfer characteristics of the three devices are compared to the measurements of Mizutani et al. in Fig. 5 for $V_{DS} = 5$ V. Good overall agreement is achieved. All simulations were conducted using the same parameter setup, except for the work-function energy difference of the gate Schottky contact (depending on the underlying material). The values for the interface charge density are summarized in Table 3. We use a positive charge at the channel/supply layer interface, a negative between the supply layer and the passivation (in the case of D-mode and recessed E-mode), a negative charge between the InGaN cap layer and the AlGaN supply layer (both E-mode devices) and a positive between the InGaN cap layer and the passivation (E-mode non-recessed).

Fig. 6 shows the effective conduction band energies of D-mode and E-mode HEMTs at $V_{GS} = 0$ V, $V_{DS} = 5$ V in a vertical cut under the gate metal, as computed by the simulator. The band diagrams are shifted, so that both Fermi levels are at 0 eV. Indeed, as suggested by Mizutani et al., a 2DEG channel is presented in the D-mode device, while the negative piezoelectric charge at the InGaN/AlGaN interface raises the conduction band in the E-mode structure. Thus, the channel is depleted even at $V_{GS} = 0$ V, and the threshold voltage increases to positive values.

Fig. 7 compares the simulated DC g_m for the three structures. The drop in the measured g_m at higher gate bias, might be due to non-idealities in the source and drain ohmic contacts, which are not considered in our simulation. A relatively good agreement between the simulated and measured output characteristics for a device with InGaN layer is achieved (Fig. 8).

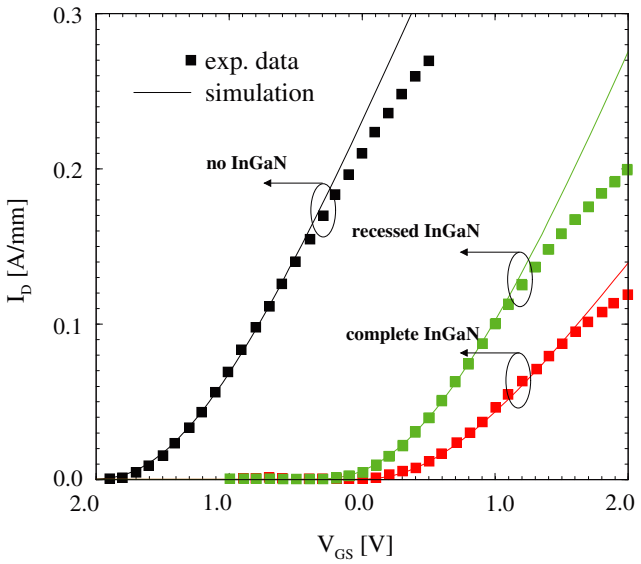

Fig. 5. Comparison of simulated and measured transfer characteristics for the three devices.

Table 3
Summary of values of interface charge density (cm^{-2})

Interface	D-mode	E-mode	Recessed E-mode
GaN/AlGaN	1×10^{13}	1×10^{13}	1×10^{13}
AlGaN/InGaN	–	-2.2×10^{13}	-2.2×10^{13}
InGaN/passivation	–	1.4×10^{13}	–
AlGaN/passivation	-0.6×10^{13}	–	-0.6×10^{13}

Small signal AC analysis using the calibrated setup delivers cut-off frequencies of $f_T = 7$ GHz for the device featuring a complete InGaN layer, and $f_T = 10$ GHz for the recessed structure, respectively. Our simulations suggest, that reasonably higher values can be achieved by shorter gate lengths: e.g. peak $f_T = 30$ GHz for $l_g = 0.8$ μm.

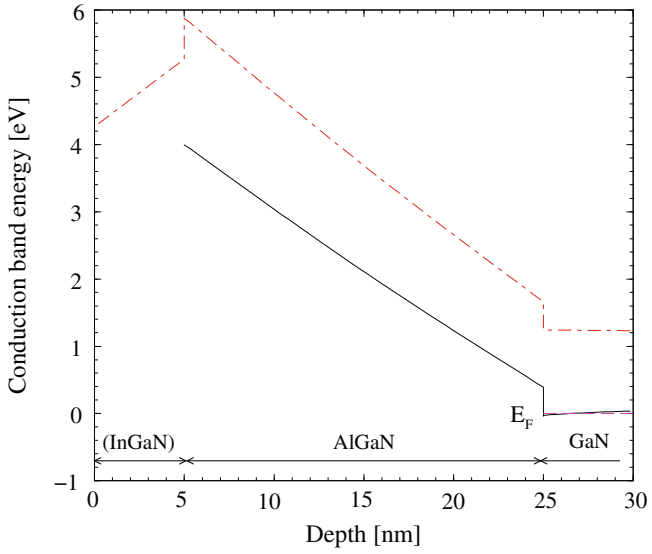

Fig. 6. Energy band diagrams of a HEMT with (dot-dashed line) and without (solid line) InGaN layer.

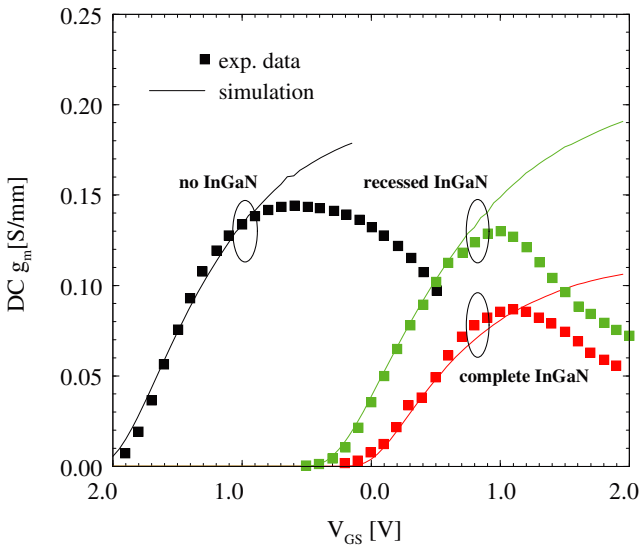

Fig. 7. Simulated DC g_m for the three devices.

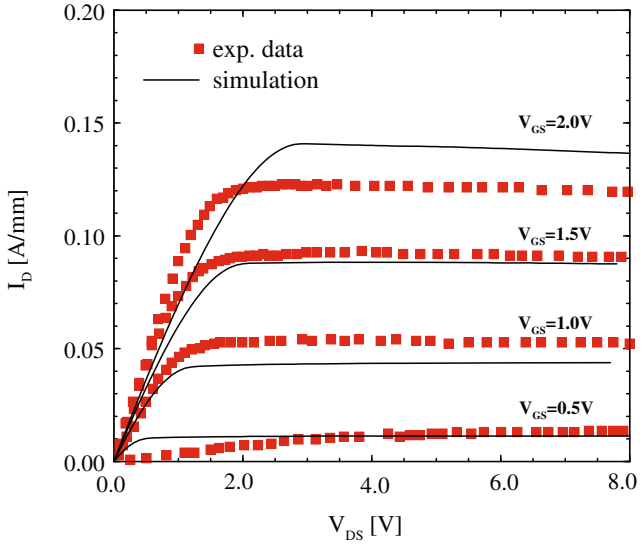

Fig. 8. Output characteristics of a HEMT with non-recessed InGaN cap layer.

5. Conclusion

A simulation study of HEMTs featuring InGaN cap layer is presented. Proper models of the material properties are proposed and several relevant physical mechanisms are accounted for. Good agreement with experimental DC data is achieved by using a calibrated parameter setup. Theoretical expectations for the AC performance are presented.

Acknowledgement

The authors acknowledge support from Austrian Science Funds (FWF), Project START Y247-N13.

References

[1] Mizutani T, Ito M, Kishimoto S, Nakamura F. AlGaN/GaN HEMTs with thin InGaN cap layer for normally off operation. IEEE Elec Dev Lett 2007;28(7):549–51.

[2] Khan M, Chen Q, Sun C, Yang J, Blasingame M, Shur M, et al. Enhancement and depletion mode GaN/AlGaN heterostructure field effect transistors. Appl Phys Lett 1996;68(4):514–6.
[3] Kumar V, Kuliev A, Tanaka T, Otoki Y, Adesida I. High transconductance enhancement mode AlGaN/GaN HEMTs on SiC substrate. Electron Lett 2003;39(24):1758–60.
[4] Cai Y, Zhou Y, Chen K, Lau K. High-performance enhancement-mode AlGaN/GaN HEMTs using fluoride-based plasma treatment. IEEE Elec Dev Lett 2005;26(7):435–7.
[5] Minimos-NT Device and Circuit Simulator. User's Guide, Release 2.0 <http://www.iue.tuwien.ac.at/mmnt>; 2002.
[6] Palankovski V, Quay R. Analysis and simulation of heterostructure devices. Wien/New York: Springer; 2004.
[7] Vitanov S, Palankovski V, Murad S, Rödle T, Quay R, Selberherr S. Predictive simulation of AlGaN/GaN HEMTs. Tech Dig IEEE Comp Semicond IC Symp 2007:131–4.
[8] Simlinger T, Brech H, Grave T, Selberherr S. Simulation of submicron double-heterojunction high electron mobility transistors with MINIMOS-NT. IEEE Trans El Dev 1997;4:700–7.
[9] Vurgaftman I, Meyer JR, Ram-Mohan R. Band parameters for III–V compound semiconductors and their alloys. J Appl Phys 2001;89:5816–47.
[10] Walukiewicz W, Lia S, Wua J, Yua K, Ager J, Hallera E, et al. Optical properties and electronic structure of InN and In-rich group III-nitride alloys. J Cryst Gr 2004;269:119–27.
[11] Seghier D, Gislason H. Dependence of the Au/AlGaN Schottky characteristics on Al content. Phys Scripta 2002;101:230–3.
[12] Jang J, Sohn S, Kim D, Seong T. Formation of low-resistance transparent Ni/Au ohmic contacts to a polarization field-induced p-InGaN/GaN superlattice. Semicond Sci Technol 2006;21:L37–39.
[13] Caughey D, Thomas R. Carrier mobilities in silicon empirically related to doping and field. Proc IEEE 1967;52:2192–3.
[14] Vitanov S, Palankovski V, Quay R, Langer E. Modeling of electron transport in GaN-based materials and devices. AIP Conf Proc: Phys Semiconduct 2007;B893:1399–400.
[15] Vitanov S, Palankovski V. Monte Carlo study of transport properties in InN. Springer Proc Phys Ser 2008;119:97–100.
[16] Hänsch W, Orlowski M, Weber W. The hot-electron problem in submicron MOSFETs. Proc 18th ESSDERC 1988:597–606.
[17] Vitanov S, Palankovski V, Murad S, Rödle T, Quay R, Selberherr S. Hydrodynamic modeling of AlGaN/GaN HEMTs. In: Proceedings of the international conference on simulation of semiconductor processes and devices. Wien/New York: Springer; 2007:273–6.